Published in final edited form as:

Cancer Res. 2017 June 15; 77(12): 3244–3254. doi:10.1158/0008-5472.CAN-16-2355.

Micellar delivery of miR-34a modulator rubone and paclitaxel in resistant prostate cancer

Di Wen[1], **Yang Peng**[1], **Feng Lin**[1], **Rakesh K. Singh**[2], and **Ram I. Mahato**[1,*]

[1]Department of Pharmaceutical Sciences, University of Nebraska Medical Center, Omaha, NE 68198

[2]Department of Pathology and Microbiology, University of Nebraska Medical Center, Omaha, NE 68198

Abstract

Treatment of prostate cancer with paclitaxel (PTX) often fails due to development of chemoresistance caused by downregulation of the tumor suppressor gene miR-34a. In this study, we demonstrate that co-delivery of PTX and 2′-hydroxy-2,4,4′,5,6′-pentamethoxychalcone (termed rubone) drives upregulation of miR-34a and chemosensitizes PTX-resistant prostate cancer cells, killing both cancer stem-like cells (CSCs) and bulk tumor cells. Rubone upregulated miR-34a and reversed its downstream target genes in DU145-TXR and PC3-TXR cells. PTX and rubone combination therapy inhibited tumor cell growth, migration, and CSC population growth. We synthesized poly(ethylene glycol)-block-poly(2-methyl-2-carboxyl-propylene carbonate-graft-dodecanol) (PEG-PCD) to prepare micelles. The drug-loading capacities were 9.70 ± 0.10% and 5.34 ± 0.02% for PTX and rubone, respectively, controlling a drug release of 60.20 ± 2.67% and 60.62 ± 4.35% release of PTX and rubone at 24 h. Delivery of miR-34a and rubone decreased PC3-TXR cell viability with increasing PTX concentration. Co-incubation with a miR-34a inhibitor diminished the effect of rubone. PTX IC50 in PC3 and PC3-TXR cells was 55.6 and 2580 nM, respectively, but decreased to 49.8 and 93.2 nM when treated in combination with rubone, demonstrating a reversal of PTX resistance by rubone. Systemic administration of micelles carrying PTX and rubone inhibited orthotopic prostate tumor growth in nude mice, compared to monotherapy, by reversing the expression of miR-34a, SIRT1, Cyclin D1 and E-cadherin. In summary, our results showed how rubone acts as an efficient small molecule modulator of miR-34a to reverse chemoresistance and further enhance the therapeutic efficacy of PTX in PTX-resistant prostate cancer.

Keywords

paclitaxel; rubone; chemoresistance; miR-34a; combination therapy

[*]**Corresponding Author:** Ram I. Mahato, Ph.D., Department of Pharmaceutical Sciences, University of Nebraska Medical Center, 986025 Nebraska Medical Center, Omaha, NE 68198, Tel: 402-559-5422; Fax: 402-559-9543, ram.mahato@unmc.edu.

Conflict of interest: No potential conflicts of interest was disclosed.

Introduction

Most prostate cancers relapse within two years into hormone refractory due to the presence of tumor initiating cells, known as cancer stem cells (CSCs), which are involved in tumor progression and metastasis, but are resistant to chemotherapy. Recently, aberrant expression of miRNAs is critically implicated in the initiation, progression, migration, and chemoresistance of cancer (1, 2). Among these miRNAs, miR-34a is significantly downregulated in chemoresistant prostate cancer cell line (3) or $CD44^+$ cancer stem cells (4). As a tumor suppressor miRNA, miR-34a is responsible for promoting tumor cell apoptosis, inhibiting tumor metastasis (5) and chemoresistance (6). Thus, miR-34a replenishment might be a novel therapeutic method to reverse PTX-resistance for the treatment of chemoresistant prostate cancer. Kojima et al. reported that miR-34a reversed PTX resistance by targeting the downstream genes including SIRT1 and Bcl-2 (7). Yao et al. reported that combination therapy using doxorubicin and miR-34a synergistically enhanced the antitumor property of doxorubicin and inhibited DU145 cell formed tumor growth *in vivo* (8). Nonetheless, intrinsic challenges associated with oligonucleotide-based miRNA replenishment including off-target effects, poor cellular uptake, and *in vivo* instability hindered its clinical translation. Even though numerous miRNA delivery systems were developed, most of them were proven less effective or toxic for clinical use (9). Thus, to reverse the aberrant expression of miR-34a by small molecules might be a potent alternative method for the treatment for PTX-resistant prostate cancer.

Natural and synthetic analogs of chalcones and isoflavones exhibit promising anticancer activity. However, only a few studies have focused on the role of chalcone derivatives on modulation of miRNAs. Rubone (10), isoliquiritigenin (11), and kuwanon V (12) modulate miR-34a, miR-25, miR-9, miR-29a and miR-181a, respectively with potent biological actions. Among these small molecules, Xiao et al. first reported rubone, a chalcone analog, as a miR-34a modulator for the inhibition of hepatocellular carcinoma (HCC) growth (10). In their study, rubone upregulated miR-34a expression in a p53 dependent manner, downregulated the downstream target Bcl-2 and Cyclin D1 expression, and suppressed HCC growth *in vivo*. However, the antitumor efficacy of rubone as a miR-34a modulator for treating PTX resistant prostate cancer and the underlining mechanisms remains largely unknown. Furthermore, poor aqueous solubility of PTX and rubone (less than 50 mg/L) results in low and variable drug absorption. Thus, novel drug delivery systems for co-delivery of both drugs are required for combination therapy against PTX resistant prostate cancer.

Since the use of solubilizing agents and surfactants may cause organ and systemic toxicity, biodegradable polymers, which can self-assemble into nano-sized micelles, are gaining much attention. Polymeric micelles have spherical structures with a hydrophilic corona and hydrophobic core, which improves the aqueous solubility and stability of hydrophobic drugs (13). The stealth property of poly(ethylene glycol) (PEG) hydrophilic corona of micelles prevents their recognition by reticuloendothelial system (RES) and therefore minimizes their rapid elimination via the enhanced permeability and retention (EPR) effect. In our previous study, we designed and synthesized poly(ethylene glycol)-*block*-poly(2-methyl-2-carboxyl-propylene carbonate-graft-dodecanol) (PEG-PCD), which significantly enhanced the

aqueous solubility of embelin, an X-linked inhibitor of apoptosis protein (XIAP) inhibitor (14). Here, we determined the effect of rubone on miR-34a and its target genes and investigated whether it could chemosensitize PTX resistant prostate cancer cells and synergistically inhibited orthotopic prostate tumor in nude mice when administered intravenously as a micellar formulation with PTX.

Materials and Methods

Cell lines and culture condition

Prostate cancer cell lines LNCaP (obtained in 2016), C4-2 (obtained in 2011), DU145 (obtained in 2010), and PC3 (obtained in 2010) were purchased from the ATCC and cultured in RPMI1640 containing 10% fetal bovine serum (FBS) and 1% penicillin/streptomycin in a humidified 37°C incubator supplemented with 5% CO_2. The PTX resistant version of DU145 and PC3 (DU145-TXR and PC3-TXR) were provided by Dr. Evan T. Keller from the University of Michigan in 2010. Normal prostate epithelial RWPE-1 cells were provided by Dr. Ming-Fong Lin from UNMC in 2016 and cultured in complete keratinocyte growth medium, K-SFM (Life Technologies) supplemented with 50 μg/mL of bovine pituitary extract and 5 ng/mL of EGF. The approximate number of passages for all cell lines between collection and thawing is 15. All cell lines were authenticated using DNA fingerprint (last time performed in 2017) by the University of Arizona Genetics Core (Tucson, AZ).

RT-PCR and Western blot analysis

Following the treatment of different concentrations of rubone or PTX and rubone combination therapy, total mRNA was isolated using RNeasy isolation kits (Qiagen, Valencia, CA) and 170 ng total RNA was converted to cDNA using miR-34a primer to determine miR-34a concentration. To determine protein concentration, cell protein was extracted using RIPA buffer after treatment with rubone at the doses of 5 and 10 μM for 48 h. The amount of protein was adjusted to the same concentration, transferred to PVDF membrane, incubated with primary and secondary antibodies, followed by Licor Odyssey system analysis (LI-COR Biotechnology, Lincoln, NE). The primary antibodies used in Western blot and immunohistochemistry studies were the following: anti-E-cadherin (Abcam, ab15148), anti-SIRT1 (Santa Cruz, sc-15404), anti-Cyclin D1 (Abcam, ab16663), anti-p53 (Santa Cruz, sc-6243), anti-Bax (Santa Cruz, sc-6236), anti-βactin (Santa Cruz, sc-1616), anti-TAp73 (Santa Cruz, sc-7957), anti-Elk-1 (Santa Cruz, sc-355).

Cell viability in 2D and 3D models

In 2D model, cell viability was determined by MTT assay after treating the cells with different concentrations of rubone or 5 μM rubone plus different concentrations of PTX. The anti-tumor effect of the combination therapy using PTX and rubone was also determined using 3D tumor model (15) including 3D on top and hanging-drop models. For 3D on top assays in 24 well plate, 200 μL of 100% Matrigel was used as the basement and 2×10^5 single cells were suspended in 300 μL 10% Matrigel in RPMI1640 as the growth medium. After culturing for 48 h, growth medium was exchanged to growth medium containing PTX and rubone at different concentrations, which was replaced with fresh media every two days for 2 weeks before analyzing the therapeutic effect. For the hanging drop model, 40 μL

medium containing 4000 cells were added in each well of 3D 96-well hanging drop plate (3D Biomatrix, Ann Arbor, MI) and drug containing medium was changed every two days for 3 weeks until sphere formation of the control group.

Cell invasion and migration

The effect of PTX and rubone combination therapy on cell invasion and migration was determined using Transwell membrane filter inserts (pore size 8 μM) in 6-well culture plates. For invasion assay, 200 μL Matrigel (BD Biosciences, CA) was added to each transwell insert where RPMI1640 without FBS was used as the cell culture medium, while RPMI1640 with 10% FBS was added in each well. PTX resistant DU145-TXR and PC3-TXR cells were cultured for another 72 h after drug treatment. The number of cells invaded Matrigel was quantified after staining with crystal violet. For migration assay, 1×10^6 cells were seeded into each transwell insert and cultured for another 72 h after adding the drugs. The cell number was counted under a microscope in randomly selected three fields after crystal violet staining for 10 minutes.

Role of CSCs in chemoresistance

We further analyzed CSC population in DU145-TXR and PC3-TXR after treatment with PTX, rubone and their combination using Aldeflour reagent (Stem Cell Technologies, Vancouver, BC) based flow cytometry. Cells were suspended in suspension media and stained by Aldeflour reagent, while a negative control comprising cells treated with ALDH-inhibitor diethylamino-benzaldehyde (DEAB) was included to gate the unspecific staining.

Polymer synthesis, micelle formulation, and characterization

Poly(ethylene glycol)-block-poly(2-methyl-2-carboxyl-propylene carbonate-graft-dodecanol) (PEG-PCD) was synthesized and characterized by ^{1}H NMR as described previously (14). PTX and rubone loaded micelles were prepared by film hydration with 10% theoretical drug loading. Chloroform was evaporated under vacuum, and resulting film was hydrated in 10 mL of phosphate buffered saline (PBS), and sonicated for 10 min using Misonix ultrasonic liquid processor (Farmingdale, NY) with an amplitude of 30, followed by removing the free drug at 5000 rpm centrifugation for 5 min. Blank or drug loaded micelles were characterized by measuring particle size using Malvern Zetasizer (Worcestershire, UK).

To determine the drug loading and encapsulation efficiency, drug loaded micelles were dissolved in 1 mL mobile phase composed of 70:30 V/V of acetonitrile and water. Concentrations of PTX and rubone were measured by reverse phase high performance liquid chromatography (RP-HPLC, Waters Milford, MA) with a UV detector at 228.6 nm for PTX and 324.3 nm for rubone using a reverse phase C18 column (250 mm×4.6 mm, Inertsil ODS). We also compared the drug loading capability of PEG-PCD with commercially available poly (ethylene glycol)-polylactide (PEG-PLA) and 1,2-distearoyl-sn-glycero-3-phosphoethanolamine-*N*-(polyethylene glycol) (DSPE-PEG) of similar molecular weights. PTX and rubone release from PEG-PCD micelles was determined after dialysis (2500–5000 Da cut off) against 50 mL PBS containing 20% ethanol as a co-solvent, which did not dissolve PEG-PCD and break the micellar structure at 37°C in a temperature controlled

shaker at the speed of 100 rpm. Sample (1 mL) was taken at specific time points (1, 2, 3, 6, 12, 24, 48, and 96 h) and replaced with 1 mL PBS containing 20% ethanol. The sample was dissolved with the mobile phase after removing the solvent using a rotary evaporator, followed by determining drug concentration using HPLC.

We further estimated the *in vivo* stability of PEG-PCD micelles using time-dependent Fluorescence Resonance Energy Transfer (FRET) in the presence of 20% FBS. 50 μg of 3,3′-dioctadecyloxacarbocyanine perchlorate (DiO) as a lipophilic fluorescent energy donor and 1,1′-dioctadecyl-3,3,3′,3′-tetramethylindocarbocyanine perchlorate (DiI) as an acceptor, 1 mg of PTX and rubone were loaded into 10 mg of PEG-PCD. Emission fluorescence spectra ranging from 490 to 590 nm was recorded at an excitation wavelength of 488 nm (donor excitation) and resulted in a strong emission at 565 nm (acceptor emission). We further compared the micelle stability of PEG-PCD with PEG-PLA and DSPE-PEG after drug loading.

In vivo tumor studies

All animal experiments were performed in accordance with the NIH animal use guideline and protocol approved by the Institutional Animal Care and Use Committee (IACUC) at the University of Nebraska Medical Center. To visualize and monitor tumor progression, we developed orthotopic prostate tumor using stably transfected prostate cancer cells with lentivirus encoding GFP and luciferase (LP-hLUC-Lv201-0200, Genecopoeia, Rockville, MD). A midline incision was made in the lower abdomen of 8 weeks old male nude mice to expose the dorsal prostate lobe, where 30 μL PBS containing 1×10^6 PC3-TXR cells expressing GFP and luciferase (PC3-TXR-GFP-Luc) were injected. Three weeks after tumor cell injection, mice with orthotopic tumor were randomly divided into six groups of 10 animals per group with administration of blank PEG-PCD micelles, PTX (20 mg/kg) loaded PEG-PCD micelles, rubone loaded PEG-PCD micelles (20 mg/kg), PTX and rubone (10 mg/kg for each drug) along, PTX and rubone loaded DSPE-PEG micelles, and PTX and rubone loaded PEG-PCD micelles. These formulations were injected intravenously for five doses every other day. The body weight and tumor luminescence of the mice were recorded once a week. Followed by the last formulation injection, four mice in each group were sacrificed and tumors were excised for determining miR-34a expression by RT-PCR. The therapeutic effect of formulation was further determined by immunohistochemistry (IHC) for Bax, Ki-67, and miR-34a downstream targets including SIRT1, E-cadherin, and Cyclin-D1. The side effects of each formulation were evaluated by hematoxylin and eosin (H&E) staining of the major organs including heart, liver, spleen, lung, and kidney. Other mice were monitored for another two weeks to further evaluate the anticancer efficacy of the formulation.

Statistical Analysis

Results were presented as the mean ± S.E.M. from three experiments for *in vitro* studies and six experiments for *in vivo* studies. The statistical difference between the two groups was calculated by unpaired Student's *t*-test, and a $P < 0.05$ was considered to be statistically significant.

Results

Rubone upregulated miR-34a and reversed the expression of miR-34a downstream targets in PTX-resistant prostate cancer cell lines

Our objective was to determine whether rubone could serve as a miR-34a modulator to reverse the miR-34a downstream tumor-associated gene expression. Thus, we first determined miR-34a expression in different prostate cancer cell lines. miR-34a expression was markedly downregulated in androgen refractory DU145, PC3, and PTX resistant DU145-TXR and PC3-TXR cells compared to androgen dependent LNCaP, LNCaP developed C4-2, as well as normal prostate epithelial RWPE-1 cells (Figure 1A), indicating the role of miR-34a in the initiation and progression of prostate cancer (16). Next, we determined the cytotoxicity of rubone in these cell lines. As shown in Figure 1B, rubone exhibited significantly higher cytotoxicity in DU145-TXR and PC3-TXR cells, suggesting that rubone had stronger anticancer effect in advanced prostate cancer cells, which had lower miR-34a expression (Figure 1A). However, rubone did not show obvious toxicity to RWPE-1, LNCaP and C4-2 cells with high miR-34a expression, indicating rubone induced cytotoxicity through miR-34a related pathways. Rubone upregulated miR-34a in PTX-resistant DU145-TXR and PC3-TXR cell lines in a dose dependent manner (Figure 1C). After evaluating the anticancer effect of rubone, we determined miR-34a downstream target gene expression after rubone treatment. PTX resistant cell lines showed more chemoresistance related SIRT1 expression (17) and less metastasis related E-cadherin expression (18) (Figure 1D and E). Rubone significantly reversed the expression of miR-34a downstream gene targets of DU145-TXR and PC3-TXR cell lines (Figure 1D and E), including E-cadherin, SIRT1, and Cyclin D1, whereas E-cadherin expression was not reversed in DU145-TXR cell line. Furthermore, rubone monotherapy promoted apoptosis determined by Bax expression in DU145-TXR and PC3-TXR cell lines. However, rubone showed less effect of reversing miR-34a downstream targets and inducing apoptosis in non-resistant DU145 and PC3 cell lines. These data indicated the downregulation of miR-34a in resistant prostate cancer and suggest that rubone might work as a specific miR-34a modulator to reverse miR-34a expression for treating androgen refractory metastatic prostate cancer.

Rubone enhanced the anticancer effect of PTX in PTX-resistant prostate cancer cell lines by reversing the expression of miR-34a downstream targets

To determine that miR-34a is an anticancer target for reversing chemoresistance of prostate cancer, we evaluated the gene regulation efficiency of miR-34a mimic and miR-34a inhibitor and their effect on PC3-TXR viability. Using lipofectamine 2000 as a transfection reagent, miR-34a mimic and inhibitor could upregulate and suppress miR-34a expression in PC3-TXR cell line, respectively (Supplementary Fig. S1A). miR-34a inhibited PC3-TXR cell viability, whereas miR-34a inhibitor promoted cell growth (Supplementary Fig. S1B). We further demonstrated that miR-34a can enhance PTX chemotherapy, whereas miR-34a inhibitor promoted cancer cell viability (Figure 2A) with PTX treatment in PC3-TXR cell line. Rubone did not enhance the anticancer effect of PTX in chemosensitive DU145 and PC3 cell lines (Figure 2B and D), but significantly reversed chemoresistance of DU145-TXR and PC3-TXR cell lines (Figure 2C and E). miR-34a inhibitor reversed the effect of

rubone on promoting PTX cytotoxicity (Figure 2F), indicating rubone promoted the effect of PTX through upregulating the expression of miR-34a. To mimic the complexity of *in vivo* tumor environment, we determined the anticancer effect of PTX and rubone in 3D tumor model. PTX and rubone combination therapy inhibited PC3-TXR cell growth and sphere formation in 3D model, including 3D on top (Figure 2G) and hanging drop model (Figure 2H). Similar to rubone monotherapy, PTX and rubone combination therapy more effectively reversed the expression of miR-34a downstream gene expression in DU145-TXR and PC3-TXR cell lines compared to non-resistant cell lines (Figure 2I and J). PTX reduced the expression of E-cadherin (19) in DU145 and PC3 cell lines, whereas PTX and rubone failed to reverse E-cadherin in DU145-TXR cell line (Figure 2I). Thus, rubone could work as a miR-34a modulator to reverse PTX-resistance in prostate cancer and restore the expression of miR-34a targeted genes.

Rubone inhibited cell invasion, migration, and CSC population in a p53-independent pathway

Treatment of prostate cancer always fails due to the metastasis and the presence of CSCs, which is highly chemoresistant (20). Thus, we further determined the effect of PTX and rubone combination therapy on the invasion and migration of DU145-TXR and PC3-TXR cells. Rubone alone or its combination with PTX significantly inhibited DU145-TXR and PC3-TXR invasion (Figure 3A and C) and migration (Figure 3B and D). Furthermore, rubone or its combination with PTX significantly downregulated aldehyde activity, which is a CSC marker (Figure 3E). Collectively, our results demonstrated that combination therapy of PTX and rubone significantly reversed chemoresistance, inhibited tumor cell migration and invasion, and decreased the CSC population of androgen refractory prostate cancer cells.

Previously research claimed that miR-34a and p53 axis regulates miR-34a expression and tumor suppression (21, 22). However, our results indicated that there was no change in p53 expression after rubone treatment, even in PC3-TXR cell line (p53 null) (Figure 1E and 2J). To determine whether rubone upregulates miR-34a in p53 independent pathways including TAp73 (23, 24) and Elk-1 (25, 26), we determined TAp73 and Elk-1 expression after rubone alone or with PTX. As shown in Figure 3F and G, rubone monotherapy or PTX and rubone combination therapy significantly enhanced TAp73 and Elk-1 expression, suggesting p53 independent pathway played a crucial role in miR-34a upregulation by rubone.

PEG-PCD micelles were effective drug delivery vehicles for PTX and rubone

Polymeric micelles have been widely used for improving the solubility and enhancing the *in vivo* stability of hydrophobic drugs. In this study, we used PEG-PCD to form micelles for co-delivery of PTX and rubone. After chemical synthesis as previously described (14), PEG-PCD polymer was characterized by ^{1}H NMR (Supplementary Fig. S2A) and the particle size distribution of micelles before and after drug loading was measured by dynamic light scattering (Supplementary Fig. S2B). PEG-PCD could form micelles with low polydispersity and drug loading did not affect the particle size. We further compared drug loading and micelle stability of PEG-PCD micelles with two commercially available polymers PEG-PLA and DSPE-PEG. After setting up standard methods of HPLC for measuring PTX and rubone concentrations, we determined the drug loading and micelle

stability of PEG-PCD, PEG-PLA, and DSPE-PEG. PEG-PCD had the highest drug loading of 9.70 ± 0.10 and 5.34 ± 0.02% for PTX and rubone (Figure 4A and B), respectively compared to PEG-PLA which showed 4.18±0.03%, 1.51±0.02%, and DSPE-PEG with 3.41 ± 0.36% and 3.58 ± 0.27%. We then determined PTX and rubone release from PEG-PCD micelles. Interestingly, PEG-PCD micelles carrying both PTX and rubone had a slower drug release profile compared to single drug loaded micelles (Figure 4C and D). At 12 h, 54.95 ± 0.90% of PTX and 61.06 ± 2.02% of rubone were released from PEG-PCD micelles with single drug loading, while 39.40 ± 0.22% of PTX and 50.13 ± 3.31% of rubone were released from PEG-PCD micelles with both drugs. We evaluated the cytotoxicity of PTX and rubone formulation on DU145-TXR and PC3-TXR cells. PEG-PCD micelles did not show cytotoxicity to each prostate cancer or normal prostate cell lines (data not shown). Micelle encapsulation decreased cytotoxicity of the combination therapy compared to free drug (Figure 4E and F) in DU145-TXR and PC3-TXR cell lines, possibly due to slow drug release from the micelles. We also determined the micelle stability by FRET assay (Supplementary Fig. S3). 20% FBS promoted the degradation and dissociation of micellar structure according to the decreased maximum relative fluorescence unit (RFU) at the wavelength of 568 nm. Micelles formed by PEG-PCD polymer exhibited higher stability compared to DSPE-PEG at each time point, but less stable than PEG-PLA after 6 h. To summarize the drug loading, release, and stability issues, PEG-PCD micelles might be an effective drug delivery system for *in vivo* PTX and rubone delivery.

PEG-PCD micellar formulation of PTX and rubone suppressed PTX-resistant prostate tumor growth *in vivo*

To monitor the tumor growth and metastasis in the orthotopic prostate cancer bearing nude mice, we first transduced PC3-TXR cell line with lentivirus expressing both GFP and luciferase. After injecting the cells into dorsal prostate lobe, tumor development was monitored by intraperitoneally injecting luciferin and recording body weight every week. We also evaluated the efficacy of PEG-PCD micelles by comparing the effect of PEG-PCD micelles with free drugs and DSPE-PEG loaded drugs. The presence and location of prostate tumor was shown in Figure 5A. The tumor inhibitory effect was demonstrated by weekly monitoring the luminescence (Figure 5B), which indicating the suppressed tumor growth in micellar combination therapy group. However, PEG-PCD micelles have better therapeutic efficacy than DSPE-PEG micelles. This orthotopic prostate cancer mouse model is very aggressive so that we observed 20% body weight loss during the treatment, while PTX and rubone formulated by PEG-PCD had little effect on body weight loss, suggesting the inhibition of tumor growth in combination therapy group (Figure 5C). Finally, all the mice were sacrificed to isolate the tumor for measuring miR-34a expression and tumor size. Rubone monotherapy or combination therapy with PTX significantly upregulated miR-34a expression in tumor (Figure 5D). Tumor luminescence and size at 7^{th} week in PEG-PCD micelles loaded PTX and rubone group were significantly lower than the other five groups (Figure 5E). To further demonstrate the anticancer mechanism of rubone *in vivo*, we isolated the tumor and determined cell proliferation marker and miR-34a downstream targets expression (Figure 6). Rubone alone or with PTX significantly reversed E-cadherin, Cyclin D1, and SIRT1 expression. Rubone monotherapy failed to suppress tumor cell proliferation as indicated by Ki-67 staining, whereas PTX and rubone combination therapy significantly

suppressed tumor cell growth compared to PTX monotherapy. We further determined TAp73 and Elk-1 expression in tumor tissue. Rubone alone or combination therapy with PTX significantly upregulated TAp73 and Elk-1 expression. These data indicated that rubone upregulated miR-34a expression in p53 independent pathways *in vivo*. Normal histology without necrosis was observed in heart and liver (Supplementary Fig. S4). There was significant decrease of hematopoiesis in spleen and acute tubular injury in kidney of PTX treated group, indicating the side effect of PTX chemotherapy. However, this side effect was reversed in PTX and rubone combination therapy group due to the decreased dose of PTX. Collectively, our results demonstrated that rubone was a potent small molecule miR-34a modulator to reverse the chemoresistance of advanced androgen-refractory prostate cancer and enhance the therapeutic effect of PTX.

Discussion

Drug resistance remains the major challenge to cancer chemotherapy even with the discovery of highly efficient anticancer compounds. Furthermore, the skeletal metastasis in advanced prostate cancer patients is the major cause of morbidity and mortality (27). Tumors are composed of bulk cancer cells and small population of CSCs, which are not responsive to most chemotherapeutic agents and result in chemoresistance and tumor recurrence (28). In recent years, miR-34a was found to inhibit CSC growth, metastasis, and chemoresistance by directly repressing the adhesion molecule CD44 (4). The downstream targets of miR-34a, including SIRT1 (29), LEF1 (30), TCF7 (31), AR, and Notch-1 (32), are crucial factors of proliferation, metastasis, and chemoresistance of advanced androgen refractory prostate cancer. Furthermore, our data indicated that miR-34a was significantly downregulated in advanced prostate cancer, especially in PTX resistant cells (Figure 1A). Thus, miR-34a replenishment by systemic delivery using nanoparticles can therefore be developed as a potent therapeutic strategy. However, the off-target effects, *in vivo* degradation, low efficacy and high cytotoxicity associated with drug delivery systems of miRNA oligonucleotide still need to be overcome for miRNA based clinical therapy.

Recently, several small molecules as oncogenic miRNA inhibitor (33, 34) and tumor suppressor miRNA modulator (10) were identified for the inhibition of tumor growth. Among these small molecules, retinoic acid (23), genistein (35), and rubone (10) have been reported to upregulate miR-34a expression in several types of cancer with the mechanism not well characterized. Traditional chemotherapy uses PTX or docetaxel as a monotherapy for inhibiting cancer cell growth, which always fails due to the chemoresistance caused by downregulation of tumor suppressor miRNA. In this study, we present an alternative strategy for fighting PTX resistant prostate cancer through miR-34a upregulation by employing a combination therapy using rubone as a small molecule miR-34a modulator. Our data suggest that rubone was non-toxic to normal prostate cells, but toxic to PTX resistant prostate cancer cells, which had low miR-34a expression (Figure 1B). For combination therapy with PTX, rubone could reverse the chemoresistance of prostate cancer at low concentration (5 μM). At this concentration, rubone significantly enhanced the cytotoxicity of PTX in PTX-resistant prostate cancer cell lines, whereas did not influence the anticancer effect of PTX in non-resistant cell lines. Extracellular matrix is key regulator of homeostasis and tissue phenotype to form 3D culture assays (36), which allows the phenotypic discrimination between

nonmalignant and malignant mammary cells. Since some crucial signals are lost when cells are cultured in vitro on 2D plastic flasks (15), 3D model could better mimic the *in vivo* tumor environment and evaluate the anticancer effect of therapeutic agents. Thus, we determined the anti-tumor efficacy of PTX and rubone combination therapy in 3D model (Figure 2G and H), where 3D on top allows the tumor to grow on extracellular matrix (Matrigel) and hanging-drop model can help tumor cell form sphere-like structure without Matrigel. PTX and rubone combination therapy inhibited tumor cell growth and disturbed tumor morphology in 3D models. These data indicated that rubone could work as a non-toxic, highly specific miR-34a modulator to enhance the therapeutic effect of PTX.

Previous report claimed that rubone inhibited HCC growth in a p53 dependent manner (10). In that research, rubone had no therapeutic effect in Hep3B cells, which did not express p53. Interestingly, our results showed that rubone significantly reversed miR-34a and its downstream target gene expression in p53-null PC3-TXR cells (Figure 2E and J). Furthermore, rubone enhanced the therapeutic effect of PTX, inhibited the metastasis, and decreased the population of CSCs in PC3-TXR cells (Figure 3A–E), suggesting that rubone might upregulate miR-34a in a p53 independent pathway. Therefore, we analyzed TAp73 (23, 24) and Elk-1 (25, 26) expression, which were previously reported to be p53 independent miR-34a regulation pathway. Our data showed that TAp73 and Elk-1 were highly upregulated after rubone monotherapy or PTX and rubone combination therapy (Figure 3F and G). This discrepancy may be explained by the extremely low expression of TAp73 (37) and Elk-1 (38) in Hep3B cells compared to PC3-TXR cells, which means that all known miR-34a regulation pathways are blocked in Hep3B cells. Thus, we conclude that rubone might work as a miR-34a modulator for prostate cancer in a p53 independent manner.

Polymeric micelles can increase aqueous solubility of hydrophobic drugs thereby avoiding the use of toxic solubilizing agents, including DMSO and Cremophor EL. In this study, we synthesized PEG-PCD lipopolymer, which allowed the conjugation of multiple lipid chains to a polycarbonate backbone for the optimization of drug loading. The pendant lipid groups in the lipopolymers could increase the interaction of hydrophobic drugs with the core, improved *in vivo* micelle stability, and prolonged circulation half-life. Thus, we compared the drug delivery property of our PEG-PCD with two commercially available polymers PEG-PLA and DSPE-PEG. PEG-PCD had higher PTX and rubone loading compared to PEG-PLA and DSPE-PEG, especially when loading both drugs (Figure 4A and B). The decreased drug release was observed when loading both drugs, indicating drug-drug interaction in the same drug delivery platform could influence the drug delivery property. Although PEG-PCD showed less stability compared to PEG-PLA, PEG-PCD had high stability at the first 6 h (Supplementary Fig. S3). By summarizing these results, PEG-PCD could be potent drug delivery platform for co-delivery of PTX and rubone.

The anticancer efficiency was evaluated in an orthotopic prostate tumor model to mimic the clinical condition and monitor tumor growth in a non-invasive manner. Tumor growth was significantly suppressed after systemic administration of PTX and rubone formulation, including DSPE-PEG and PEG-PCD micelles, compared with other four groups according to the luminescence at each time point (Figure 5B) and the tumor size at the end of the study

(Figure 5E). PEG-PCD micelles delivered PTX and rubone more efficiently suppressed tumor growth and reversed miR-34a expression compared to free drug and DSPE-PEG micelles, probably because PEG-PCD micelles had better drug loading (Figure 4A and B) and stability (Supplementary Fig. S3). This can be explained by the chemical structure of PEG-PCD with multiple dodecanal lipid chains attached to the polycarbonate backbone, which could enhance the hydrophobic interaction among the hydrophobic cores. However, DSPE-PEG only has two lipid chains per PEG molecule. Our data also indicated that PTX and rubone combination therapy reversed the downstream target genes of miR-34a through TAp73 and Elk-1 pathways (Figure 6). However, this orthotopic model using PC3-TXR cell line was very aggressive since we observed severe body weight loss in the progress of tumor (Figure 5C) and few mice could survive for more than 7 weeks without treatment. Under this severe condition, PTX and rubone combination therapy showed promising therapeutic effect by suppressing the tumor growth and avoid body weight loss. Furthermore, our formulations did not show severe organ toxicity in heart and liver, and combination therapy reversed the side effect of PTX on hematopoiesis in spleen and acute tubular injury in kidney (Supplementary Fig. S4). In some liver and spleen slides of PTX treated groups, we also observed foamy histiocytes and kupffer cells full of lipids, which was diminished in combination therapy group (Supplementary Fig. S4).

Based on our results, rubone could be a specific miR-34a regulator to reverse miR-34a and the downstream target gene expression for PTX resistant prostate cancer (Figure 7). The replenished miR-34a enhanced the anticancer effect of PTX on microtubule disarray, which promoted cell apoptosis and inhibits proliferation. Moreover, this miR-34a replenishment by rubone was in a p53 independent manner in DU145-TXR and PC3-TXR cell lines. PTX and rubone combination therapy formulated by PEG-PCD micelles could significantly suppress PTX resistant tumor growth *in vivo*. This study illustrated the therapeutic potency of rubone as a small molecule miR-34a modulator for the treatment of PTX-resistant prostate cancer.

Supplementary Material

Refer to Web version on PubMed Central for supplementary material.

Acknowledgments

We would like to appreciate the help from Dr. Geoffrey Talmon and Dr. Yuri. Sheinin from the University of Nebraska Medical Center for analyzing the tissue slides.

Financial support: D. Wen, Y. Peng, F. Lin, R. K. Singh, and R. I. Mahato were supported by the faculty start-up fund from the University of Nebraska Medical Center to R. I. Mahato.

References

1. Croce CM. Causes and consequences of microRNA dysregulation in cancer. Nat Rev Genet. 2009; 10(10):704–14. [PubMed: 19763153]
2. Esquela-Kerscher A, Slack FJ. Oncomirs – microRNAs with a role in cancer. Nat Rev Cancer. 2006; 6(4):259–69. [PubMed: 16557279]
3. Singh S, Chitkara D, Mehrazin R, Behrman SW, Wake RW, Mahato RI. Chemoresistance in prostate cancer cells is regulated by miRNAs and hedgehog pathway. PLoS One. 2012; 7(6):e40021. [PubMed: 22768203]

4. Liu C, Kelnar K, Liu B, et al. The microRNA miR-34a inhibits prostate cancer stem cells and metastasis by directly repressing CD44. Nat Med. 2011; 17(2):211–5. [PubMed: 21240262]
5. Wang G, Liu G, Ye Y, Fu Y, Zhang X. Upregulation of miR-34a by diallyl disulfide suppresses invasion and induces apoptosis in SGC-7901 cells through inhibition of the PI3K/akt signaling pathway. Oncol Lett. 2016; 11(4):2661–7. [PubMed: 27073535]
6. Fujita Y, Kojima K, Hamada N, et al. Effects of miR-34a on cell growth and chemoresistance in prostate cancer PC3 cells. Biochem Biophys Res Commun. 2008; 377(1):114–9. [PubMed: 18834855]
7. Kojima K, Fujita Y, Nozawa Y, Deguchi T, Ito M. MiR-34a attenuates paclitaxel-resistance of hormone-refractory prostate cancer PC3 cells through direct and indirect mechanisms. Prostate. 2010; 70(14):1501–12. [PubMed: 20687223]
8. Yao C, Liu J, Wu X, et al. Reducible self-assembling cationic polypeptide-based micelles mediate co-delivery of doxorubicin and microRNA-34a for androgen-independent prostate cancer therapy. J Control Release. 2016
9. Wen D, Danquah M, Chaudhary AK, Mahato RI. Small molecules targeting microRNA for cancer therapy: Promises and obstacles. J Control Release. 2015; 219:237–47. [PubMed: 26256260]
10. Xiao Z, Li CH, Chan SL, et al. A small-molecule modulator of the tumor-suppressor miR34a inhibits the growth of hepatocellular carcinoma. Cancer Res. 2014; 74(21):6236–47. [PubMed: 25217526]
11. Wang Z, Wang N, Liu P, et al. MicroRNA-25 regulates chemoresistance-associated autophagy in breast cancer cells, a process modulated by the natural autophagy inducer isoliquiritigenin. Oncotarget. 2014; 5(16):7013–26. [PubMed: 25026296]
12. Kong SY, Park MH, Lee M, et al. Kuwanon V inhibits proliferation, promotes cell survival and increases neurogenesis of neural stem cells. PLoS One. 2015; 10(2):e0118188. [PubMed: 25706719]
13. Wen D, Chitkara D, Wu H, et al. LHRH-conjugated micelles for targeted delivery of antiandrogen to treat advanced prostate cancer. Pharm Res. 2014; 31(10):2784–95. [PubMed: 24789451]
14. Li F, Danquah M, Mahato RI. Synthesis and characterization of amphiphilic lipopolymers for micellar drug delivery. Biomacromolecules. 2010; 11(10):2610–20. [PubMed: 20804201]
15. Lee GY, Kenny PA, Lee EH, Bissell MJ. Three-dimensional culture models of normal and malignant breast epithelial cells. Nat Methods. 2007; 4(4):359–65. [PubMed: 17396127]
16. Kopczynska E. Role of microRNAs in the resistance of prostate cancer to docetaxel and paclitaxel. Contemp Oncol (Pozn). 2015; 19(6):423–7. [PubMed: 26843836]
17. Kojima K, Ohhashi R, Fujita Y, et al. A role for SIRT1 in cell growth and chemoresistance in prostate cancer PC3 and DU145 cells. Biochem Biophys Res Commun. 2008; 373(3):423–8. [PubMed: 18573234]
18. Fan L, Wang H, Xia X, et al. Loss of E-cadherin promotes prostate cancer metastasis via upregulation of metastasis-associated gene 1 expression. Oncol Lett. 2012; 4(6):1225–33. [PubMed: 23205121]
19. Lou PJ, Chen WP, Lin CT, Chen HC, Wu JC. Taxol reduces cytosolic E-cadherin and beta-catenin levels in nasopharyngeal carcinoma cell line TW-039: Cross-talk between the microtubule- and actin-based cytoskeletons. J Cell Biochem. 2000; 79(4):542–56. [PubMed: 10996845]
20. Li F, Mahato RI. MicroRNAs and drug resistance in prostate cancers. Mol Pharm. 2014; 11(8): 2539–52. [PubMed: 24742219]
21. Okada N, Lin CP, Ribeiro MC, et al. A positive feedback between p53 and miR-34 miRNAs mediates tumor suppression. Genes Dev. 2014; 28(5):438–50. [PubMed: 24532687]
22. Menges CW, Kadariya Y, Altomare D, et al. Tumor suppressor alterations cooperate to drive aggressive mesotheliomas with enriched cancer stem cells via a p53-miR-34a-c-met axis. Cancer Res. 2014; 74(4):1261–71. [PubMed: 24371224]
23. Agostini M, Tucci P, Killick R, et al. Neuronal differentiation by TAp73 is mediated by microRNA-34a regulation of synaptic protein targets. Proc Natl Acad Sci U S A. 2011; 108(52): 21093–8. [PubMed: 22160687]

24. Busuttil V, Droin N, McCormick L, et al. NF-kappaB inhibits T-cell activation-induced, p73-dependent cell death by induction of MDM2. Proc Natl Acad Sci U S A. 2010; 107(42):18061–6. [PubMed: 20921405]
25. Frigo DE, Duong BN, Melnik LI, et al. Flavonoid phytochemicals regulate activator protein-1 signal transduction pathways in endometrial and kidney stable cell lines. J Nutr. 2002; 132(7): 1848–53. [PubMed: 12097658]
26. Christoffersen NR, Shalgi R, Frankel LB, et al. p53-independent upregulation of miR-34a during oncogene-induced senescence represses MYC. Cell Death Differ. 2010; 17(2):236–45. [PubMed: 19696787]
27. Nandana S, Chung LW. Prostate cancer progression and metastasis: Potential regulatory pathways for therapeutic targeting. Am J Clin Exp Urol. 2014; 2(2):92–101. [PubMed: 25374910]
28. Collins AT, Berry PA, Hyde C, Stower MJ, Maitland NJ. Prospective identification of tumorigenic prostate cancer stem cells. Cancer Res. 2005; 65(23):10946–51. [PubMed: 16322242]
29. Duan K, Ge YC, Zhang XP, et al. miR-34a inhibits cell proliferation in prostate cancer by downregulation of SIRT1 expression. Oncol Lett. 2015; 10(5):3223–7. [PubMed: 26722316]
30. Liang J, Li Y, Daniels G, et al. LEF1 targeting EMT in prostate cancer invasion is regulated by miR-34a. Mol Cancer Res. 2015; 13(4):681–8. [PubMed: 25587085]
31. Chen WY, Liu SY, Chang YS, et al. MicroRNA-34a regulates WNT/TCF7 signaling and inhibits bone metastasis in ras-activated prostate cancer. Oncotarget. 2015; 6(1):441–57. [PubMed: 25436980]
32. Kashat M, Azzouz L, Sarkar SH, Kong D, Li Y, Sarkar FH. Inactivation of AR and notch-1 signaling by miR-34a attenuates prostate cancer aggressiveness. Am J Transl Res. 2012; 4(4):432–42. [PubMed: 23145211]
33. Bose D, Jayaraj G, Suryawanshi H, et al. The tuberculosis drug streptomycin as a potential cancer therapeutic: Inhibition of miR-21 function by directly targeting its precursor. Angew Chem Int Ed Engl. 2012; 51(4):1019–23. [PubMed: 22173871]
34. Vo DD, Staedel C, Zehnacker L, Benhida R, Darfeuille F, Duca M. Targeting the production of oncogenic microRNAs with multimodal synthetic small molecules. ACS Chem Biol. 2014; 9(3): 711–21. [PubMed: 24359019]
35. Chiyomaru T, Yamamura S, Fukuhara S, et al. Genistein inhibits prostate cancer cell growth by targeting miR-34a and oncogenic HOTAIR. PLoS One. 2013; 8(8):e70372. [PubMed: 23936419]
36. Bissell MJ, Radisky DC, Rizki A, Weaver VM, Petersen OW. The organizing principle: Microenvironmental influences in the normal and malignant breast. Differentiation. 2002; 70(9–10):537–46. [PubMed: 12492495]
37. Wang J, Xie H, Gao F, Zhao T, Yang H, Kang B. Curcumin induces apoptosis in p53-null Hep3B cells through a TAp73/DNp73-dependent pathway. Tumour Biol. 2016; 37(3):4203–12. [PubMed: 26490992]
38. Yue CH, Huang CY, Tsai JH, et al. MZF-1/elk-1 complex binds to protein kinase calpha promoter and is involved in hepatocellular carcinoma. PLoS One. 2015; 10(5):e0127420. [PubMed: 26010542]

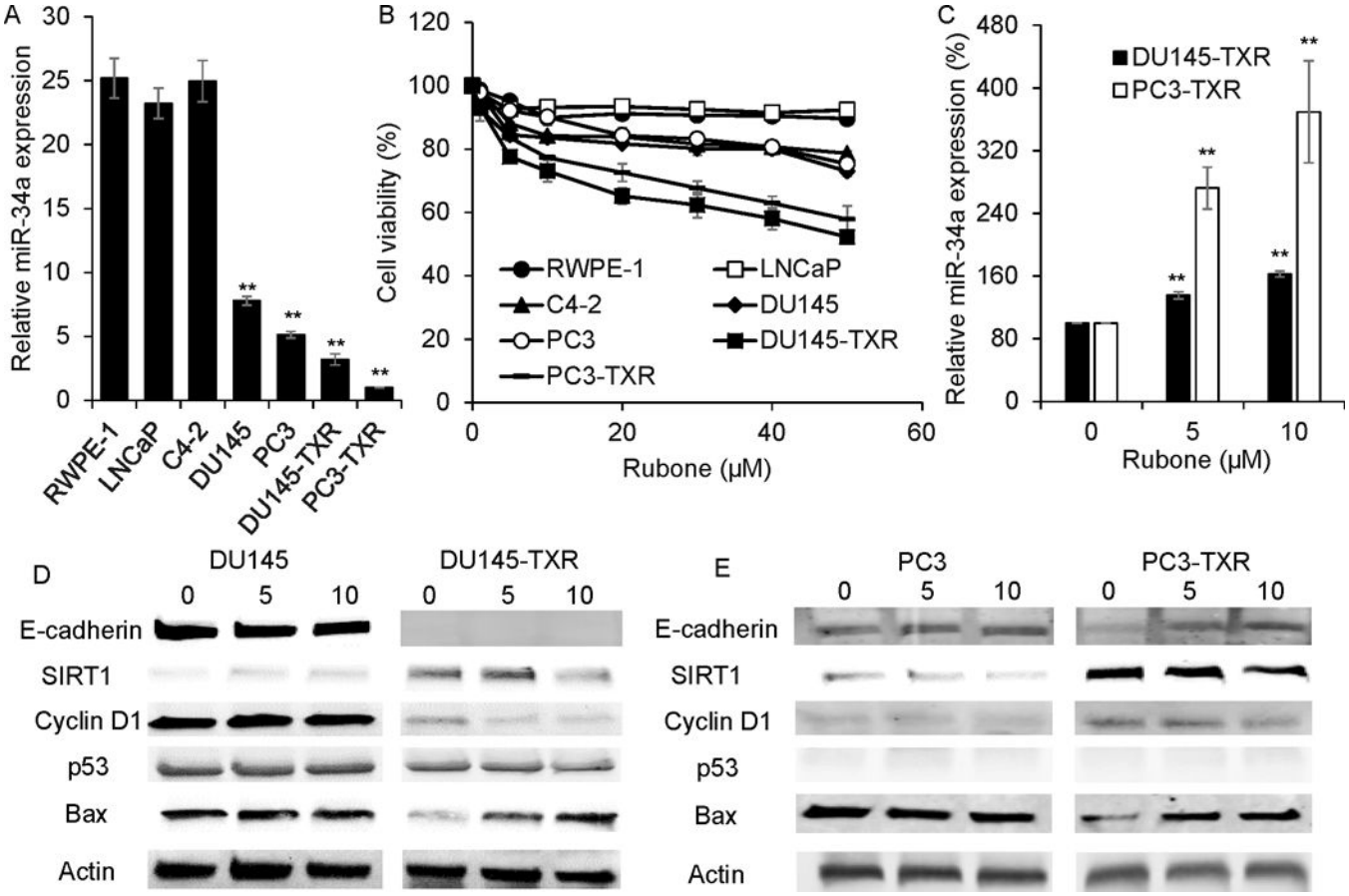

Figure 1.

Effect of rubone monotherapy on miR-34a expression. A. miR-34a expression in prostate cancer and normal prostate cell lines (Student t test; **p < 0.01 vs. RWPE-1 cell, respectively, n = 3). B. Cytotoxicity of rubone on prostate cancer and normal prostate cell lines. C. Rubone upregulated miR-34a expression in DU145-TXR and PC3-TXR in a dose dependent manner (Student t test; **p < 0.01 vs. Rubone 0 μM, respectively, n = 3). Rubone alone reversed the expression of miR-34a downstream proteins in DU145 (D) and PC3 (E) cell lines.

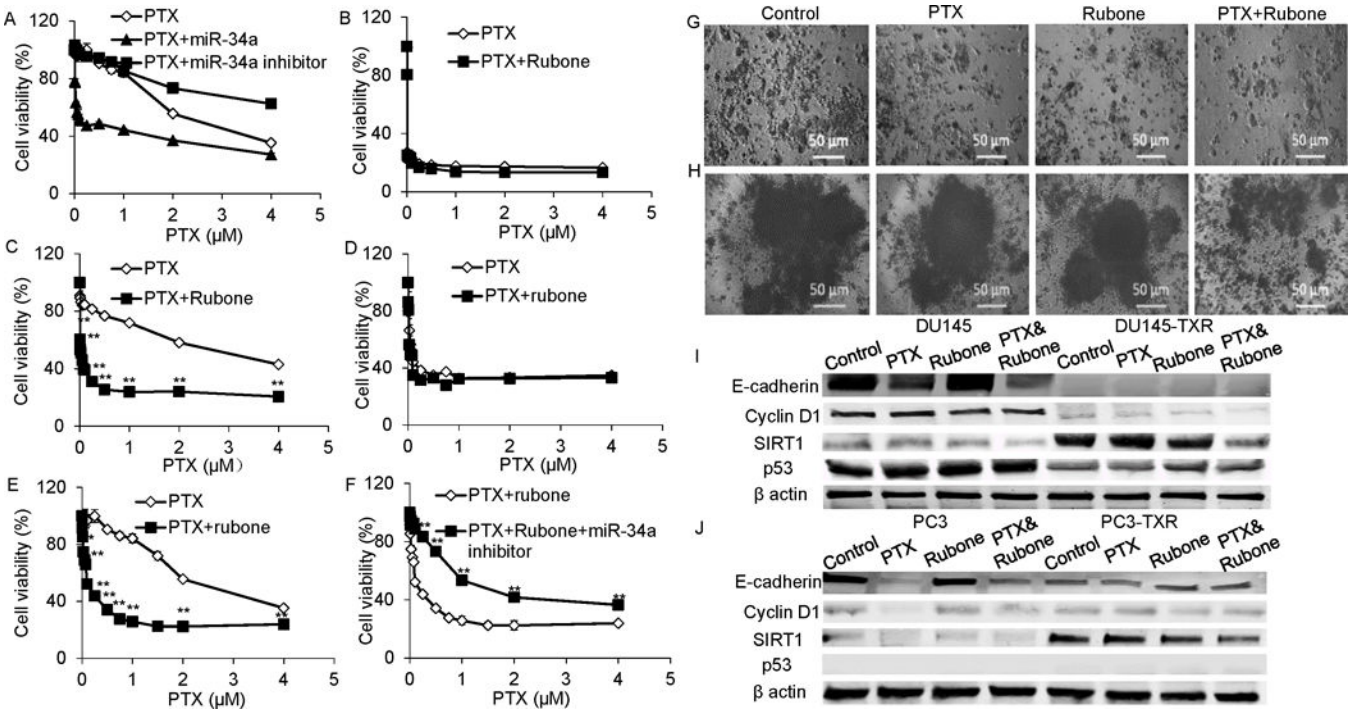

Figure 2.

Effects of PTX and rubone combination therapy on PTX resistant cell viability. A. Cell viability of PC3-TXR cells after PTX, PTX+miR-34a, and PTX+miR-34a inhibitor treatment. DU145 (B), DU145-TXR (C), PC3 (D), PC3-TXR (E) cell viability was determined by MTT assay after PTX or PTX and rubone combination therapy. (Student t test; **p < 0.01 vs. PTX at each concentration, respectively, n = 3) F. Cell viability of PC3-TXR cells after PTX+rubone and PTX+rubone + miR-34a inhibitor treatment (Student t test; **p < 0.01 vs. PTX+rubone at each concentration, respectively, n = 3).PC3-TXR cell viability and sphere formation after rubone or PTX and rubone combination therapy was determined by 3D tumor model (G, 3D on top; H, hanging drop). PTX and rubone combination therapy reversed the expression of miR-34a downstream proteins in DU145 (I) and PC3 (J) cell lines.

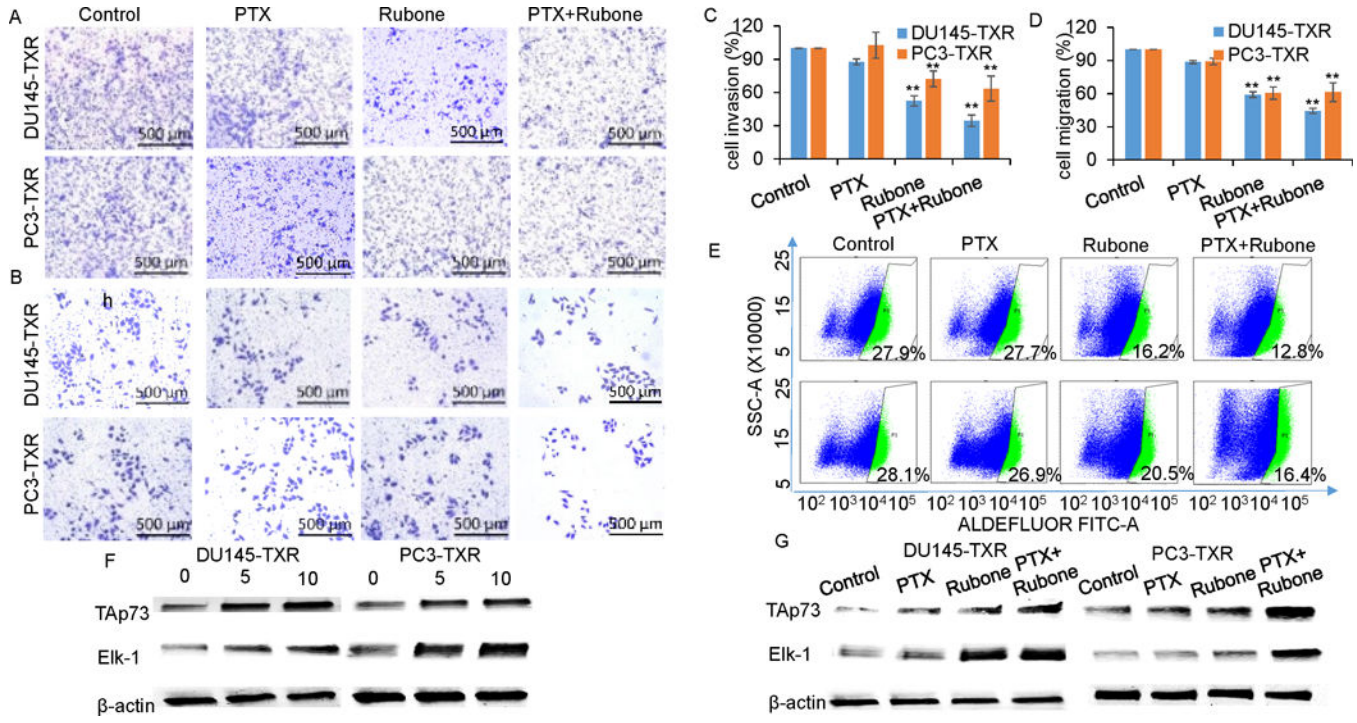

Figure 3.

PTX and rubone combination therapy inhibit cell migration, invasion, and CSC population in p53 independent manner. The effect of rubone monotherapy or PTX and rubone combination therapy on tumor cell invasion (A, upper line, DU145-TXR; bottom line, PC3-TXR) and migration (B, upper line, DU145-TXR; bottom line, PC3-TXR) were determined by crystal violet staining and quantified (C, invasion; D, migration) (Student t test; $^{**}p < 0.01$ vs. control, respectively, n = 3). E. CSC population were analyzed by Aldefluor staining and quantified by flow cytometry (upper line, DU145-TXR; bottom line, PC3-TXR). PTX and rubone combination therapy reversed miR-34a downstream protein expression of DU145 and PC3 cell lines in p53 independent manner. Rubone alone (F) or with PTX (G) upregulated Tap73 and ELK-1 expression.

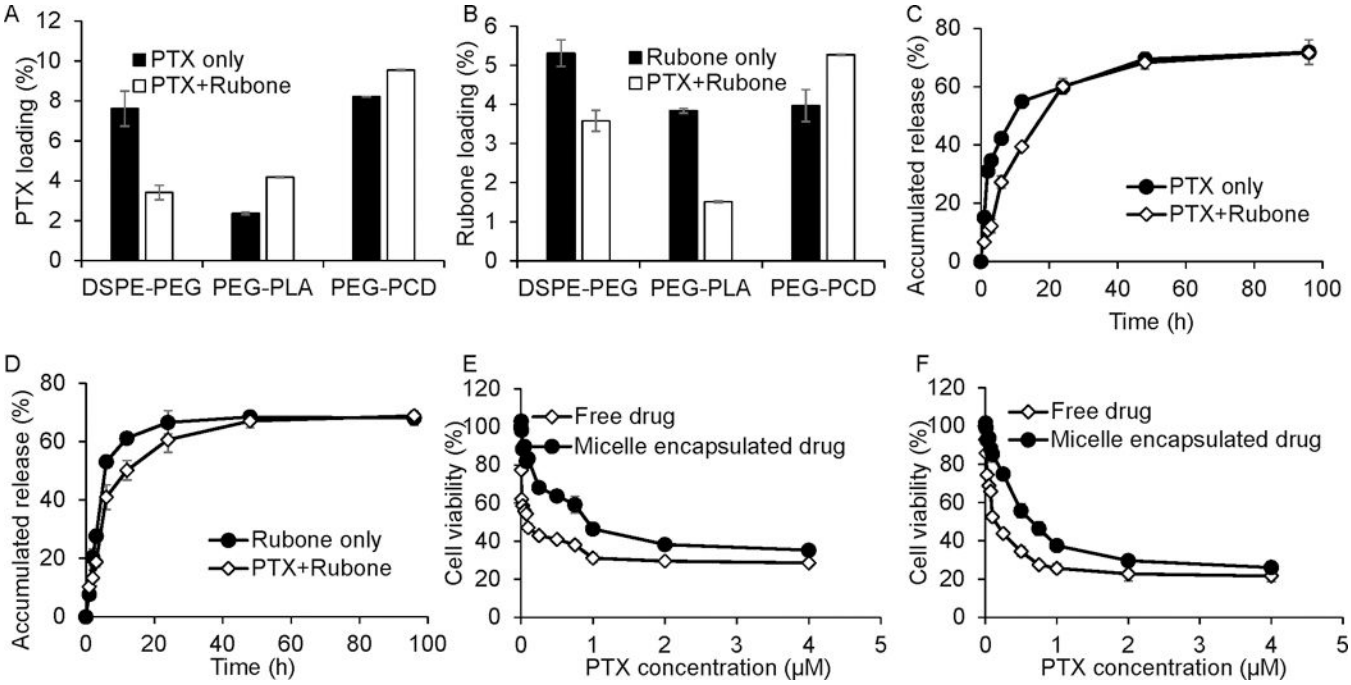

Figure 4.

Characterization of PEG-PCD micelles. PTX and rubone loading of DSPE-PEG, PEG-PLA, and PEG-PCD were measure by HPLC using standard curve of PTX and rubone. PTX and rubone loading were summarized in A and B for PTX and rubone, respectively. PTX (C) and rubone (D) release profile in single drug loaded micelles or PTX and rubone loaded micelles were determined by HPLC. The effect of PEG-PCD encapsulation on drug toxicity was determined in DU145-TXR (E) and PC3-TXR (F) cell lines.

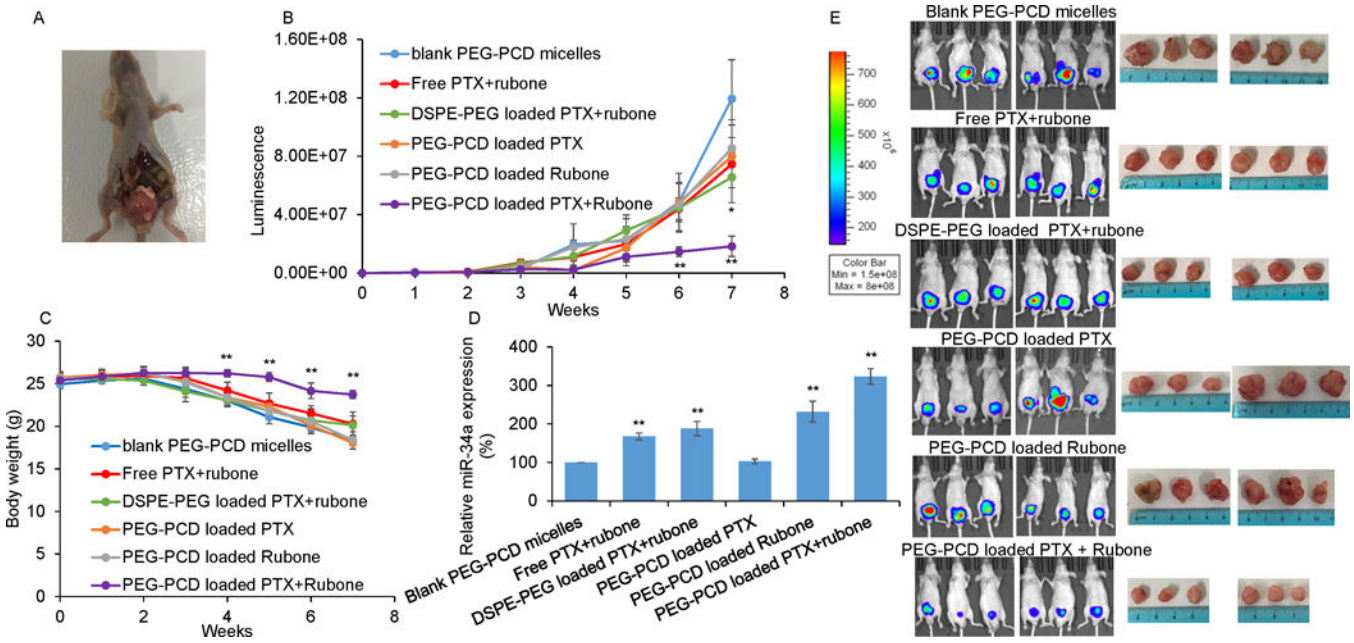

Figure 5.

Anti-tumor efficacy of PTX and rubone combination therapy. Orthotopic prostate cancer model was generated using luciferase expressed PC3-TXR cell line. Drug formulation was injected every two days after 3 weeks. A. Location of orthotopic tumor generated from PC3-TXR cell. B. In vivo tumor luminescence was determined by intraperitoneal injection of luciferin (120 mg/kg) (Student t test; *p<0.05, **p < 0.01 vs. Blank micelles, n = 6). C. Body weight of mice in each group (Student t test; **p < 0.01 vs. blank micelles, n = 6). D. miR-34a expression in tumor was determined by RT-PCR (Student t test; **p < 0.01 vs. blank micelles, respectively, n = 3). E. Bioluminescence and size of tumors in each group after 7 weeks.

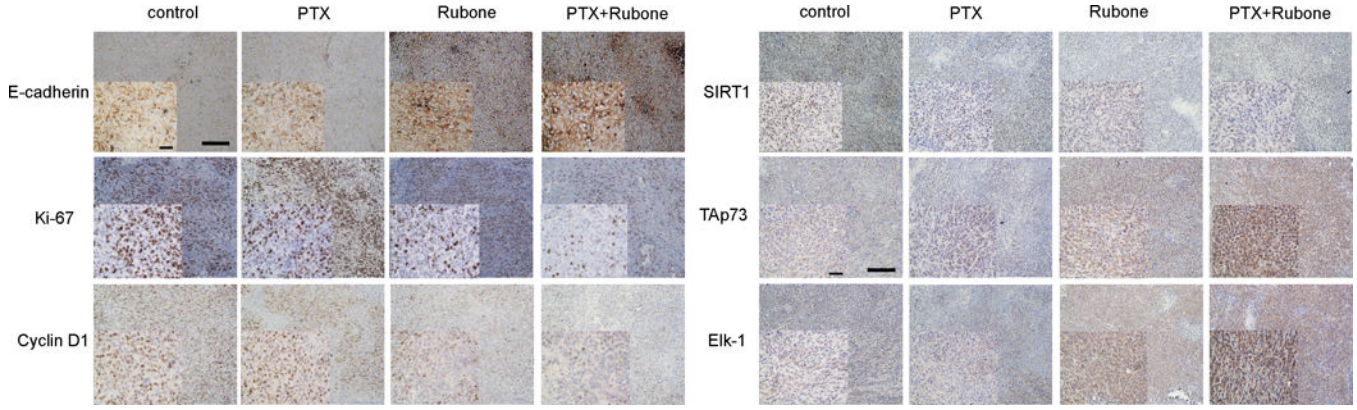

Figure 6.

Mechanism of miR-34a regulation in vivo. E-cadherin, Ki-67, cyclin D1, SIRT-1, Tap73, and Elk-1 expression after PTX and rubone formulation therapy was determined by IHC (Scale bar, 200 μM for backward figure and 50 μM for enlarged figure).

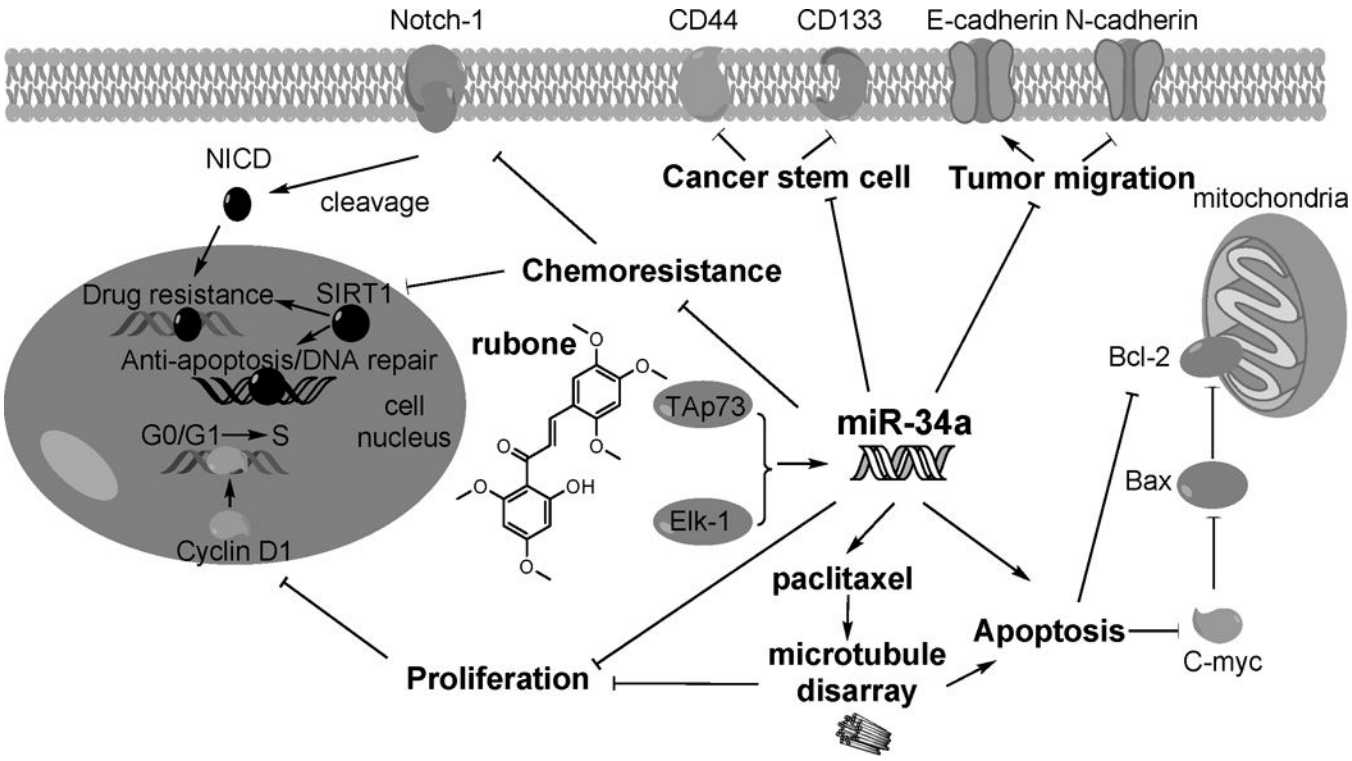

Figure 7.
Illustration of rubone working as a miR-34a modulator for combination therapy with PTX.